



# Systemic delivery of biotherapeutic RNA to the myocardium transiently modulates cardiac contractility in vivo

Vladimir V. Shuvaev<sup>a,1</sup> , Ying K. Tam<sup>b</sup>, Benjamin W. Lee<sup>c</sup>, Jacob W. Myerson<sup>a</sup>, Alan Herbst<sup>d</sup> , Raisa Yu. Kiseleva<sup>a,2</sup>, Patrick M. Glassman<sup>a,e</sup> , Hamideh Parhiz<sup>a,f</sup>, Mohamad-Gabriel Alameh<sup>f</sup>, Norbert Pardi<sup>f,3</sup> , Hiromi Muramatsu<sup>f,3</sup> , Tea I. Shuvaeva<sup>a</sup> , Evguenia Arguiri<sup>a</sup>, Oscar A. Marcos-Contreras<sup>a</sup> , Elizabeth D. Hood<sup>a</sup> , Taylor V. Brysgel<sup>a</sup> , Jia Nong<sup>a</sup> , Tyler E. Papp<sup>f</sup>, Deborah M. Eaton<sup>c</sup>, Rachel Riley<sup>g,4</sup>, Rohan Palanki<sup>g</sup> , Kiran Musunuru<sup>c</sup>, Jacob S. Brenner<sup>h</sup>, Michael J. Mitchell<sup>g</sup> , Victor A. Ferrari<sup>c</sup>, Barbara L. Mui<sup>b</sup>, Sean C. Semple<sup>b</sup>, Sherry A. Weppler<sup>b</sup> , Pavan Atluri<sup>d</sup> , Kenneth B. Margulies<sup>c</sup> , Drew Weissman<sup>f</sup> , and Vladimir R. Muzykantov<sup>a,1</sup>

Affiliations are included on p. 9.

Edited by Daniel G. Anderson, Massachusetts Institute of Technology, Cambridge, MA; received May 8, 2024; accepted June 16, 2025 by Editorial Board Member Rakesh K. Jain

**Lipid nanoparticles (LNP) represent a versatile platform for improving delivery of therapeutic nucleic acids. Yet, delivery to the myocardium remains a formidable challenge due to local barriers in the heart and systemic hindrances. In particular, plasma apolipoprotein E (apoE) directs LNP to the liver, limiting potential extrahepatic delivery. Here, we report a cardiotropic LNP (cLNP), which within 30 min post-intravenous injection accumulates in the heart of ApoE knockout (*ApoE*<sup>-/-</sup>) mice. The findings were confirmed for *ApoE*<sup>-/-</sup> rats and for wild-type mice after siRNA-mediated plasma apoE ablation. To test cardiac-specific functional effects as a proof of concept, we used cLNP loaded with siRNA to *ATP2A2*, encoding the sarcoplasmic-endoplasmic reticulum Ca<sup>2+</sup> ATPase 2a (SERCA2A). This cardiomyocyte-specific protein is a key regulator of contractility and relaxation. Intravenous administration of cLNP/siRNA-ATP2A2 in *ApoE*<sup>-/-</sup> mice led to near-complete ablation of SERCA2A in the myocardium and a potent modulation of contractility of the cardiomyocytes obtained from these mice. In summary, cardiotropic nanocarriers may allow the delivery and effect of RNA and other agents to the myocardium. Achieving this unmet medical need promises new types of treatment for heart diseases, which remains the leading cause of death worldwide.**

lipid nanoparticles | cardiac drug delivery | siRNA | SERCA2 | mRNA

Heart pathologies, including acute myocardial infarction, heart failure, fibrosis, and arrhythmias, are the leading cause of death worldwide (1). Despite advances in treatment of some cardiologic conditions, their prevalence is increasing, mortality and morbidity are high, and quality of life for survivors is often poor (2, 3). Most approved cardiac drugs act at remote sites (e.g., kidneys), with indirect or secondary cardiac effects. Biologics offering direct engagement of molecular targets within the cardiomyocyte can modify contractile deficits in the failing heart; however, these require abundant delivery to the myocardium. Indeed, poor delivery to the heart has been demonstrated in clinical trials and is a major obstacle to cardiac gene therapy (4). Novel drug delivery systems (DDS) are required to make effective nucleotide-based therapies to the heart possible.

The heart is an especially challenging drug target. It pumps through its chambers the entire blood volume in a minute, but blood components do not transfer from the blood to the endocardium. Structural (i.e. tight stable endothelial junctions), biomechanical (i.e. systole-assisted lymphatic drainage), and diffusional (i.e. densely packed bundles of cardiomyocytes in the myocardial tissue) factors minimize net extravasation and assure rapid clearance of the interstitial space to prevent myocardial edema. These limit selective accumulation of DDS in the heart (5). Even DDS injected directly into the beating heart muscle are rapidly cleared from the organ (6). DDS extravasation in the heart via leaky vessels in ischemia and other pathologies is very limited. Further, in acute myocardial infarction (AMI), flow cessation obliterates vascular delivery of cardiac DDS to affected areas (7–9). Therefore, DDS with cardiac targeting must overcome the vascular, interstitial, and cellular barriers to exert its desired function.

Attempts to design cardiac DDS have been insufficient. Use of DDSs coated with ligands binding to the extracellular matrix may enhance tissue retention, but not intracellular delivery. DDSs for active targeting use ligands of “heart-specific” epitopes and carriers with “natural heart tropism” (e.g., AAV9, cells, cell fragments, protein complexes, etc.). They bind to, enter, and exert effects in cardiac cells in vitro, but these models have limited to in vivo results impact (10). Cardiac uptake of “targeted” exosomes exceeded

## Significance

We demonstrate a drug delivery system based on lipid nanoparticles that effectively accumulate in the heart of mice and rats and are able to reach cardiomyocytes after intravenous administration into *ApoE*<sup>-/-</sup> mice. Reported results show high efficacy of molecular interventions directed to one of the most challenging targets, the myocardium. Cardiotropic lipid nanoparticles are expected to emerge as a platform for cardiac delivery of diverse cargoes to achieve effective therapeutic, diagnostic, and prophylactic interventions in the heart.

Competing interest statement: Y.K.T., B.L.M., S.C.S. and S.A.W. are employees of Acuitas Therapeutics, Y.K.T. and B.L.M. hold equity in Acuitas Therapeutics, D.W., V.R.M., and V.V.S. have filed a patent application based on some aspects of this work.

This article is a PNAS Direct Submission. D.G.A. is a guest editor invited by the Editorial Board.

Copyright © 2025 the Author(s). Published by PNAS. This article is distributed under [Creative Commons Attribution-NonCommercial-NoDerivatives License 4.0 \(CC BY-NC-ND\)](https://creativecommons.org/licenses/by-nc-nd/4.0/).

<sup>1</sup>To whom correspondence may be addressed. Email: shuvaev@penmedicine.upenn.edu or muzykant@penmedicine.upenn.edu.

<sup>2</sup>Present address: Century Therapeutics, LLC, Philadelphia, PA 19104.

<sup>3</sup>Present address: Department of Microbiology, Perelman School of Medicine, University of Pennsylvania, Philadelphia, PA 19104.

<sup>4</sup>Present address: Department of Bioengineering, Rowan University, Glassboro, NJ 08028.

This article contains supporting information online at <https://www.pnas.org/lookup/suppl/doi:10.1073/pnas.2409266122/-/DCSupplemental>.

Published July 16, 2025.

control by ~15% (11–16). The heart-to-liver ratio of “targeted” protein complexes was 0.014 *vs.* 0.007 in controls (17–19). The two-fold difference is impressive, but the low absolute value limits the utility. The cardiac uptake of DDSs is generally orders of magnitude inferior to hepatic uptake (12, 15, 17). A recent review stated: “critical assessment of the results so far achieved indicates that the efficiency of cardiac gene delivery remains a major hurdle preventing success,” and also noted that “the nonpolar and hydrophobic nature of the cardiac sarcolemma represents a formidable barrier to negatively charged nucleic acids” (20).

The success of nucleoside-modified mRNA in COVID-19 vaccines given to billions of people (21, 22), FDA-approved siRNA in ONPATRO<sup>®</sup> to treat hereditary transthyretin-mediated amyloidosis (6, 22–27) and the results of multitudes of clinical and animal studies demonstrate that lipid nanoparticles (LNP) represent a versatile type of nanocarrier for delivery of nucleic acid-based drugs (22, 24, 25). Numerous LNP iterations have emerged for targeting cargoes to desirable cells, tissues, and organs in the body. Using ligands with specific affinity to targets (28–30) and screening LNP libraries to identify variants featuring fortuitous tropism to sites of interest (31–34) represent major approaches in this area of research (31, 35–37).

Apolipoprotein E (apoE) is a component of plasma lipoproteins that has an affinity for several apoE receptors, such as LDLR and LRP1. It directs lipoprotein to cells expressing these receptors, i.e., hepatocytes and macrophages (38). ApoE is rapidly acquired by intravenously injected LNP driving LNP hepatic uptake (32). The liver is lavishly perfused via a network of fenestrated vessels enabling contact of the agents circulating in blood with hepatocytes in the parenchyma and macrophages in the sinuses (39, 40). Due to these factors, the liver takes the largest share of most types of LNP and other DDSs. Extrahepatic targeting is an area of active

investigation including apoE ablation as a useful tool to decrease liver uptake and to reveal LNP extrahepatic tropisms otherwise blocked by fast liver clearance (41). Nevertheless, extrahepatic delivery remains a major challenge in the tissue delivery field, including heart delivery (42).

Here, we report the finding of a cardiotropic LNP (cLNP) that demonstrates the following properties after IV injection in apoE-depleted (e.g., *ApoE*<sup>-/-</sup>) animals. A) Within 30 min, it accumulates in the normal heart at a level of 30–40% of injected dose per gram of tissues (%ID/g). B) Biological activity of siRNA in cLNP manifests activity in myocardial parenchymal cells, i.e. cardiomyocytes (CMCs). C) This delivery strategy enables the RNA cargo to exert expected transient alterations in the cardiac contractile function in normal animals.

## Results

**Observation of Cardiotropic LNP Accumulation in the Heart of ApoE-Depleted Animals.** Isotope tracing of cLNP labeled with <sup>3</sup>H-cholesteryl hexadecyl ether (<sup>3</sup>H-CHE) described in prior publications (43–45) demonstrated that 30 min post-IV administration, cLNP predominantly distributed to the liver and spleen in WT mice and uptake in these organs were, respectively, 3.4- and 5.8-fold lower in *ApoE*<sup>-/-</sup> mice (Fig. 1A). In other organs, uptake of cLNP was minimal across both strains, with one unexpected exception, the heart (Fig. 1A). Thirty min post-IV administration, cardiac uptake of cLNP was an order of magnitude higher in *ApoE*<sup>-/-</sup> *vs.* WT mice (38.3 ± 9.6 *vs.* 5.4 ± 1.3 %ID/g), with a heart-to-liver ratio (HLR) 41 times higher in *ApoE*<sup>-/-</sup> mice compared to WT (Fig. 1A).

Moreover, both direct detection of cLNP ionizable cationic lipid by LC-MS/MS and tracing of cLNP labeled with <sup>125</sup>I

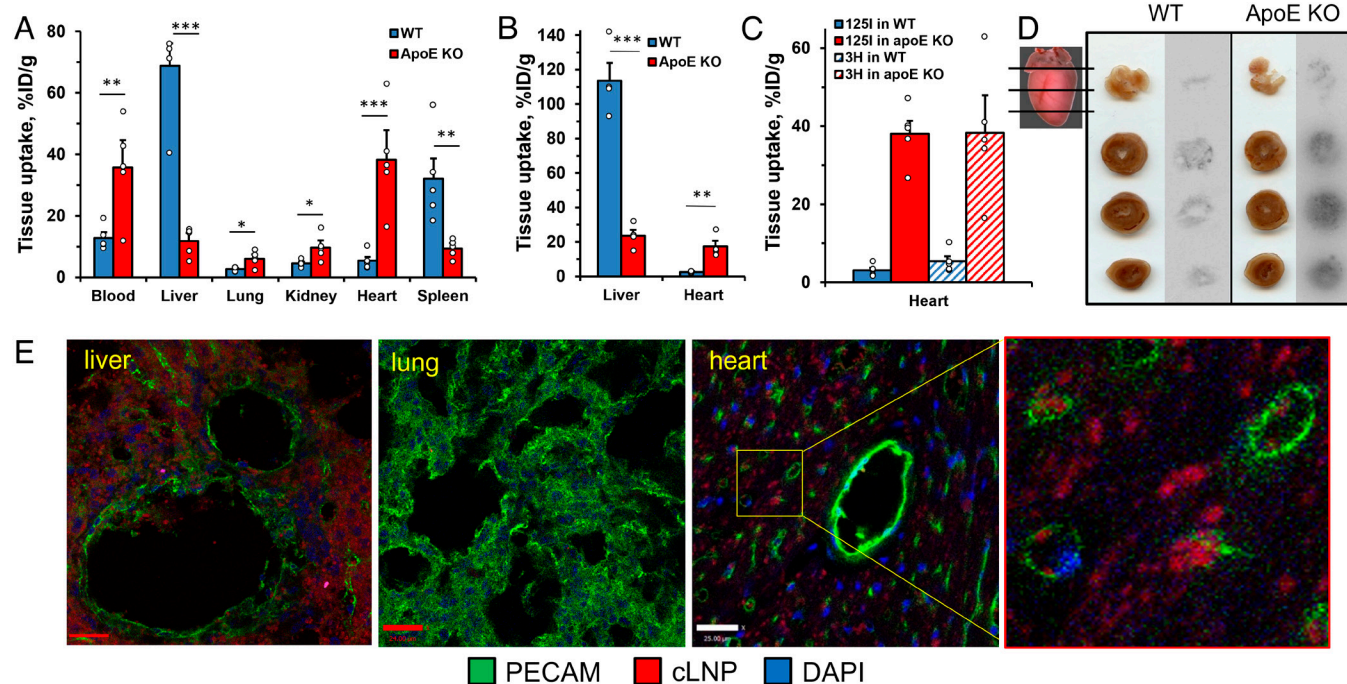


**Fig. 1.** Observation of cLNP accumulation in the heart. (A) <sup>3</sup>H-CHE-cLNP (1 μg of RNA/mouse) tissue distribution in WT *vs.* *ApoE*<sup>-/-</sup> mice 30 min post-IV administration, *n* ≥ 5. (B) cLNP level in the liver and heart 30 min post-IV measured by LC-MS/MS of ionizable aminolipid. *n* = 4. (C) Comparison of cLNP uptake in the heart of WT *vs.* *ApoE*<sup>-/-</sup> mice traced by <sup>125</sup>I-<sup>3</sup>H-CHE labels. (D) Autoradiography of the mouse heart 30 min post-IV administration <sup>125</sup>I-cLNP (scheme illustrates the approximate position of 2-mm heart slices). (E) Confocal microscopy of the liver, lung, and heart obtained from *ApoE*<sup>-/-</sup> mice 30 min post-IV administration of PKH26-labeled cLNP (bar = 25 μm). Alexa Fluor 647-labeled anti-PECAM/CD31 antibody were injected 10 min before killing of mice to denote vascular endothelium. Right panel: Expanded part of the micrograph shows cLNP in the extravascular area of the myocardium. Unless stated otherwise, blue *vs.* red denote WT *vs.* *ApoE*<sup>-/-</sup> mice, respectively. *n* = 3 to 5 biologically independent animals (A–C and E). Data are shown as M ± SEM, \**P* < 0.05; \*\**P* < 0.01; \*\*\**P* < 0.001 (*t* test or two-way ANOVA with Tukey’s post hoc test).

isotope showed similar elevation of cardiac uptake in *ApoE*<sup>-/-</sup> vs. WT mice (Fig. 1 *B* and *C* and *SI Appendix*, Fig. S1). Autoradiographic images visualized accumulation of <sup>125</sup>I-labeled cLNP in the myocardium of *ApoE*<sup>-/-</sup> mice (Fig. 1*D*). Confocal microscopy demonstrated that 30 min post-IV injection in *ApoE*<sup>-/-</sup> mice, uptake of fluorescently labeled cLNP was high in the liver, marginal in the lungs, and abundant in the heart (Fig. 1*E* and *Movies S1* and *S2*). Staining of endothelial cells with PECAM-1/CD31 antibody revealed that cLNP in the heart were localized predominantly with bundles of cardiomyocytes in the myocardial parenchyma (Fig. 1 *E*, *Inset*).

To explore the generalizability of our finding that cLNPs accumulate in the hearts of *ApoE*<sup>-/-</sup> mice, we tested the biodistribution of cLNPs following injection into alternative model systems. We observed that cLNP accumulated in the heart of *ApoE*<sup>-/-</sup> rats (*SI Appendix*, Fig. S2*A* and *F*). Moreover, transient depletion of plasma apoE in WT mice by apoE-specific siRNA (*SI Appendix*, Fig. S2*B*) caused similar cLNP accumulation in the heart (*SI Appendix*, Fig. S2*C*). To check the direct role of apoE in withholding the cardiotropic feature of cLNP, the particles were pretreated with mouse apoE and injected into *ApoE*<sup>-/-</sup> mice. cLNP pretreatment with apoE significantly augmented hepatic uptake and decreased uptake by the heart (*SI Appendix*, Fig. S2*D*) to the level close to WT. Since *ApoE*<sup>-/-</sup> mice may accumulate some lipid abnormalities with aging, we compared cLNP uptake by the heart in animals of different ages (46). The age of *ApoE*<sup>-/-</sup> mice did not affect LNP cardiotropism (*SI Appendix*, Fig. S2*E*). Taken together the results confirmed that cLNP heart accumulation was caused by apoE ablation rather than confounding lipid abnormalities that may develop in *ApoE*<sup>-/-</sup> mice.

**Pharmacologic Features of Cardiotropic LNP.** LNP are highly versatile types of carriers. Their content, method of assembly, and, in some cases, the features of the cargo affect the structure and properties of the LNP (31, 37, 41, 47, 48). We observed both homopolymer poly-C-loaded cLNP and empty (RNA-free) cLNP were equally cardiotropic (Fig. 2*A*). In contrast, cLNP increased in size from 80 to 350 nm failed to accumulate in the heart (Fig. 2*B*). Moreover, LNPs with other ionizable lipids tested in the study did not show such heart accumulation (Fig. 2*C* and *SI Appendix*, Fig. S3) indicating a unique property of cLNP. The liver and spleen are organs of clearance for many types of nanomaterials after intravenous administration. Our comparison of several LNPs showed significant variability of tissue distribution. For example, several tested LNPs such as MC3 and DOTAP showed high splenic uptake while cLNP uptake by the spleen was moderate in WT animals. Moreover, apoE depletion caused significant loss of splenic uptake of cLNP and SM-102 suggesting a significant role of apoE in the process. In contrast, high splenic uptake of MC3 and DOTAP was apoE independent (*SI Appendix*, Fig. S3).

Pharmacokinetic studies in *ApoE*<sup>-/-</sup> mice showed that radiolabeled cLNP (1 μg/mouse, 40 μg/kg) was gradually cleared from the blood, while cardiac uptake rapidly increased to a peak at 30 min (i.e., 10-fold increase from the level at 5 min) following by tissue clearance (Fig. 2*D*). It is of note that the kinetics of the cardiac uptake of radiolabeled cLNP was markedly faster (max level at 30 min post-IV) than the kinetics of functional activity of the cargo, such as siRNA, suggesting degradation or loss of the traced lipid moieties of cLNP after their delivery of RNA cargo. Similar patterns were observed in *ApoE*<sup>-/-</sup> rats (*SI Appendix*, Fig. S2*E*).

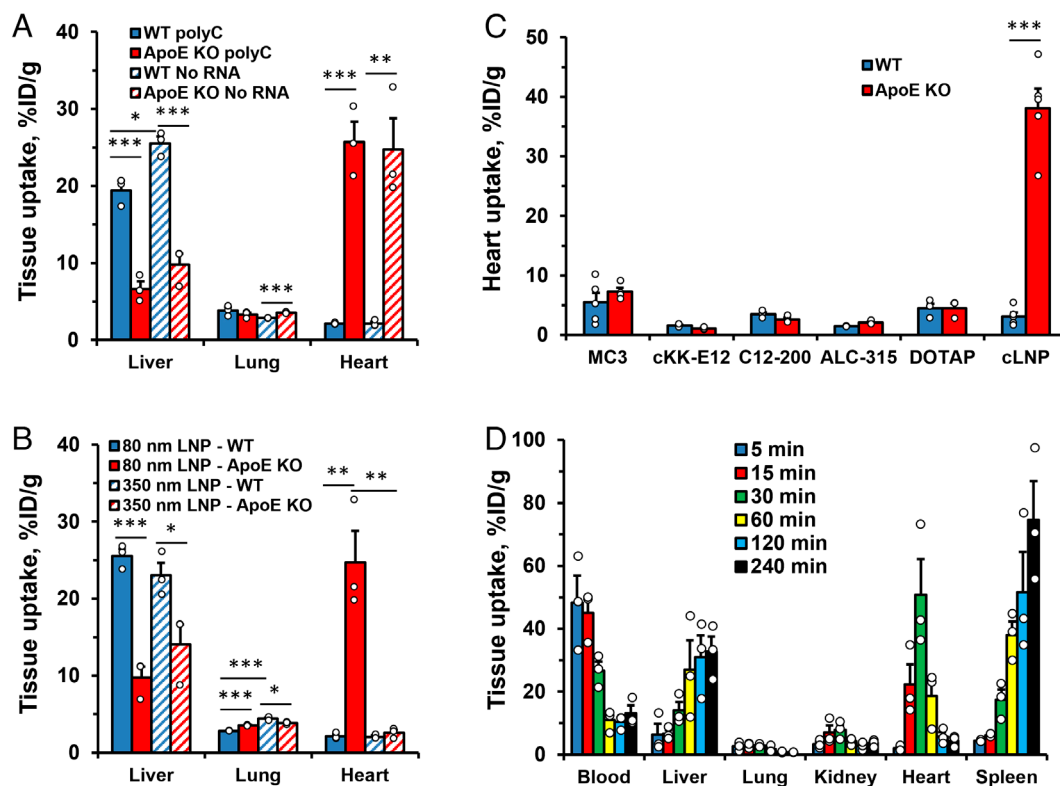


**Fig. 2.** Pharmacological properties of cardiotropic cLNP. (*A* and *B*) <sup>125</sup>I-labeled cLNP tissue distribution in WT vs. *ApoE*<sup>-/-</sup> mice 30 min post-IV administration. (*A*) Empty cLNP vs. poly-C RNA-loaded cLNP. (*B*) 80-nm cLNP vs. 350 nm cLNP. (*C*) Heart uptake of LNPs formulated with indicated ionizable lipids in comparison with cLNP. (*D*) Pharmacokinetics of <sup>3</sup>H-CHE-cLNP injected in *ApoE*<sup>-/-</sup> mice and organs were perfused with 10 mL of PBS and harvested at indicated times. Data are shown as Mean ± SEM, \**P* < 0.05; \*\**P* < 0.01; \*\*\**P* < 0.001 (*t* test or two-way ANOVA with Tukey's post hoc test).

**cLNP Pharmacokinetics and Biodistribution.** The proposed physiologically based pharmacokinetic (PBPK) model was able to simultaneously describe the differences in PBPK between WT and *ApoE*<sup>-/-</sup> mice based solely on differences in plasma ApoE expression. Model-fitted profiles of WT PK, *ApoE*<sup>-/-</sup> PK, and *ApoE*<sup>-/-</sup> dose-ranging biodistribution are shown in *SI Appendix, Fig. S4*. Estimated parameters are shown in *SI Appendix, Table S2*. Differences in the saturable cardiac uptake pathway between strains were described using unique  $K_m$  values for each strain. The model estimated that the “affinity” for the heart in this pathway was 10.5-fold lower in WT mice, as compared to *ApoE*<sup>-/-</sup> mice. For the liver and spleen, the ApoE-dependent clearance pathway was only included in WT mice and the parallel elimination pathway was the sole route of tissue uptake in *ApoE*<sup>-/-</sup> mice. All other parameters were shared between strains. Using visual inspection of the decline slopes of cLNP from organs, it was noted that the heart had substantially faster elimination of the labeled component of the LNP and the spleen had much slower elimination than other organs. This was described in the model using tissue-specific elimination rate constants.

**Target Engagement of Systemic cLNP/Atp2a2-siRNA Delivery.**

As an initial exploration of the functional impact of cLNP in the heart, we generated an siRNA cargo against *Atp2a2* encoding SERCA2A, a specific calcium ATPase/channel in the sarcoplasmic reticulum of CMC. In vitro activity of the siRNA was confirmed by a 90% reduction of mRNA transcript, and significant reduction of protein with correlated functional responses in induced pluripotent stem cell-derived cardiomyocytes (*SI Appendix, Fig. S5*). siRNA was then packaged into cLNP and injected intravenously (10 μg/mouse, 0.4 mg/kg) to *ApoE*<sup>-/-</sup> mice (Fig. 3*A*). By 3 d following cLNP/Atp2a2-siRNA delivery, we observed near-complete loss

of SERCA2 protein in the myocardium that recovered by day 5 (Fig. 3*B*). Immunofluorescent staining confirmed loss of SERCA2 protein in cardiomyocytes (*SI Appendix, Fig. S6*). We observed that the loss of SERCA2 correlated with compensatory heart enlargement and a transient increase in CMC cross-sectional area without overt myocardial inflammation or injury (Fig. 3*C–E* and *SI Appendix, Fig. S7*). Injection of cLNP bearing scrambled siRNA did not lead (at 24 h) to changes in heart weight or microscopic myocardial morphology (*SI Appendix, Fig. S8*).

**cLNP/Atp2a2-siRNA Modulates Cardiomyocyte Contractility.**

SERCA2A is primarily responsible for reuptake of calcium into the sarcoplasmic reticulum following cardiac contraction and is a key regulator of cardiac contraction and relaxation (Fig. 4*A*). 3 d following intravenous cLNP/siRNA injection, at the nadir of SERCA2 expression, CMCs were isolated and contractility assessed. CMCs from animals injected with cLNP/Atp2a2-siRNA had significantly reduced fractional shortening and slower departure and return velocities, consistent with SERCA2 inhibition in CMCs (Fig. 4*B*). Control scrambled cLNP/siRNA yielded no anatomic or functional changes to the heart or isolated CMCs compared to untreated. The effect of cLNP/siRNA was not a nonspecific effect of the presence of foreign RNA since in vitro transfection of isolated rat cardiomyocytes with cLNP carrying mRNA-GFP demonstrated increased green fluorescence without impacting contractility (*SI Appendix, Fig. S9*).

These data demonstrated that IV injected cLNP/siRNA: A) caused specific and potent modulation of SERCA2A cardiomyocyte gene expression; B) manifested functional effects in the heart consistent with targeted delivery, uptake, and activity in CMCs and, C) caused no overt nonspecific toxicities. The results provided

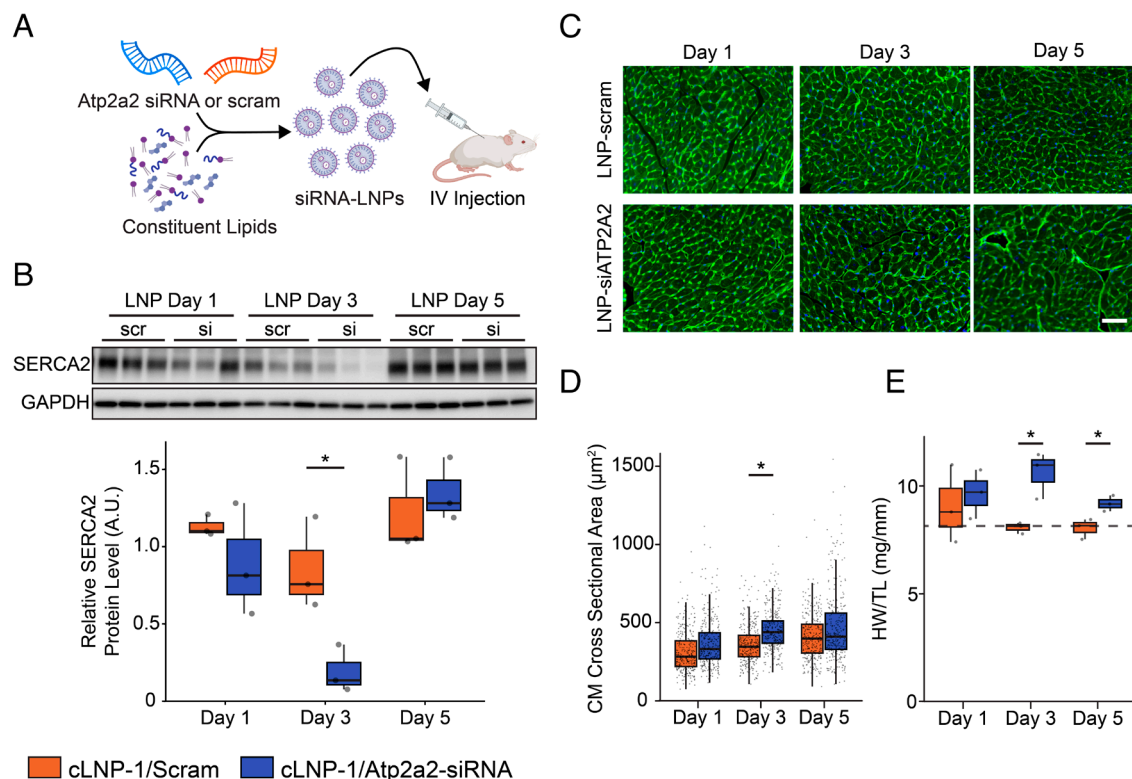


**Fig. 3.** Cardiac delivery of cLNP/Atp2a2 siRNA. (A) *Atp2a2* siRNA-loaded cLNP were IV injected into *ApoE*<sup>-/-</sup> mice and SERCA2 level was detected in a 5-d time course. (B) Immunoblot of heart protein isolates 1, 3, or 5 d following 10 μg cLNP/siRNA injection, for SERCA2 relative to GAPDH, with associated densitometry (n = 3, \*P < 0.05). (C) Representative CMC cross sections stained for cell membranes with wheat-germ agglutinin (green), and nuclei with DAPI (blue), and (D) associated quantitation of CMC cross-sectional area (N = 3 animals per group, n = 100 CMCs per animal, boxes show the median and 25th and 75th percentiles, \*P < 0.01). (E) Heart weight (HW) relative to tibia length (TL) (n = 3, the dashed line represents average HW/TL in uninjected controls; boxes show the median and 25th and 75th percentiles, \*P < 0.05).

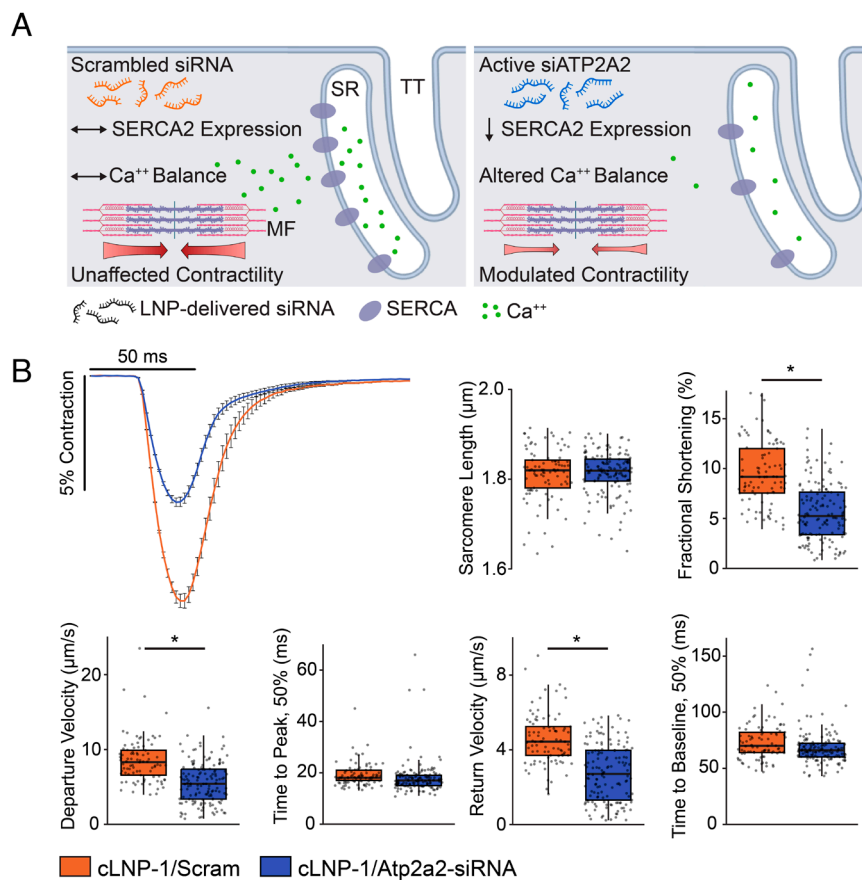


**Fig. 4.** cLNP/Atp2a2-siRNA modulates cardiomyocyte contractility. (A) Proposed activity of siRNA-Atp2a2. (B) Measurement of sarcomere shortening in CMCs isolated from mice 3 d after cLNP/siRNA injection. Note reduced fractional shortening, slowed contraction, and relaxation kinetics cLNP/siRNA-treated group ( $*P < 0.05$ ) Average  $\pm$  s.e.m. traces of sarcomere shortening, and associated contraction and relaxation parameters averaged over 6 to 10 transients during pacing at 1 Hz (N = 3 animals per group, n = 22 to 49 CMCs per animal). Boxes show the median and 25th and 75th percentiles,  $*P < 0.05$ .

proof of therapeutic feasibility for targeting CMCs with cLNP/RNA in vivo. Thus, cLNPs can pass endothelium, reach CMCs, and deliver their active cargo to the cytosol compartment.

**cLNP/Cre-mRNA Delivery to Cardiomyocytes.** To confirm that cLNP can deliver an active mRNA cargo to CMCs, we used Cre recombinase mRNA-LNP in mTmG mice (Fig. 5A). Mice were pretreated with apoE siRNA-LNP to transiently deplete plasma apoE and then injected with Cre mRNA-cLNP or Cre mRNA-SM102-LNP as a noncardiotropic control (Fig. 5B and C). The confocal microscopy results demonstrated that the treatment was effective and both LNPs transformed almost all liver cells (Fig. 5D, Lower panels), as anticipated due to high nanoparticle uptake by the liver even in *ApoE*<sup>-/-</sup> mice. However, we observed significantly more gene editing of CMCs by the cLNP vs. SM102 LNP ( $28.1 \pm 1.6$  vs.  $6.2 \pm 1.8\%$ , respectively;  $P < 0.001$ ) (n = 3 animals per group) (Fig. 5D, Top panels). Future development of cLNPs will optimize the delivery of mRNA using cLNPs, as has been performed with other cell types and LNP formulations (49).

**cLNP Toxicity Studies.** Further, we embarked on the initial appraisal of unintended effects of cLNP in animals. Activation of the host defense and immune systems represents a relatively common side effect of the DDS including LNPs. Accordingly, we measured the blood level of cytokines, mediators, and markers of proinflammatory changes 24, 48, and 72 h after injection in apoE-ablated mice of cLNP (0.4 mg/kg) vs. FDA-approved LNP based on MC3. The results showed that compared with LPS used as positive control, both MC3 LNP and cLNP caused a modest

increase in the blood level of MCP-1 and IL-6 (SI Appendix, Table S4). All other 11 tested cytokines were not changed and stayed at a basal level (the range is close to the background, which explains high variability). Thus, the data showed that despite modest inflammatory response to cLNP it was no higher than that of FDA-approved MC3 LNP.

## Discussion

The heart is an important locus for pharmacotherapies, but it is very difficult to deliver drugs and especially nucleic acids that require intracellular delivery to specific cell types. Currently, no DDS enters and acts in the myocardium effectively and specifically (6, 26, 27) other than direct RNA injection into the myocardium that stimulates angiogenesis (50). Targeting intravenous agents to the heart *via* vascular epitopes may be a more attractive strategy than passive delivery. Previously used formulations included antibody-coated liposomes, tannic acid-linked protein complexes, and cardiotropic exosomes. They were found to bind, be taken up by, and exert effects in cardiac cells in vitro (11–16, 18, 51–53). Alas, very few of the DDSs showing promise in cell cultures in vitro significantly accumulate in the heart in vivo (10). Further, delivery of most, if not all DDSs, is impeded by hepatic uptake outcompeting cardiac uptake by orders of magnitude (12, 15, 17). The cLNP reported here demonstrates selective tropism to the heart (Figs. 1 and 4) in the absence of apoE, regardless of the method of ApoE depletion and across multiple species.

We demonstrate that intravenous administration of cLNP leads to a rapid accumulation in the heart followed by an effective

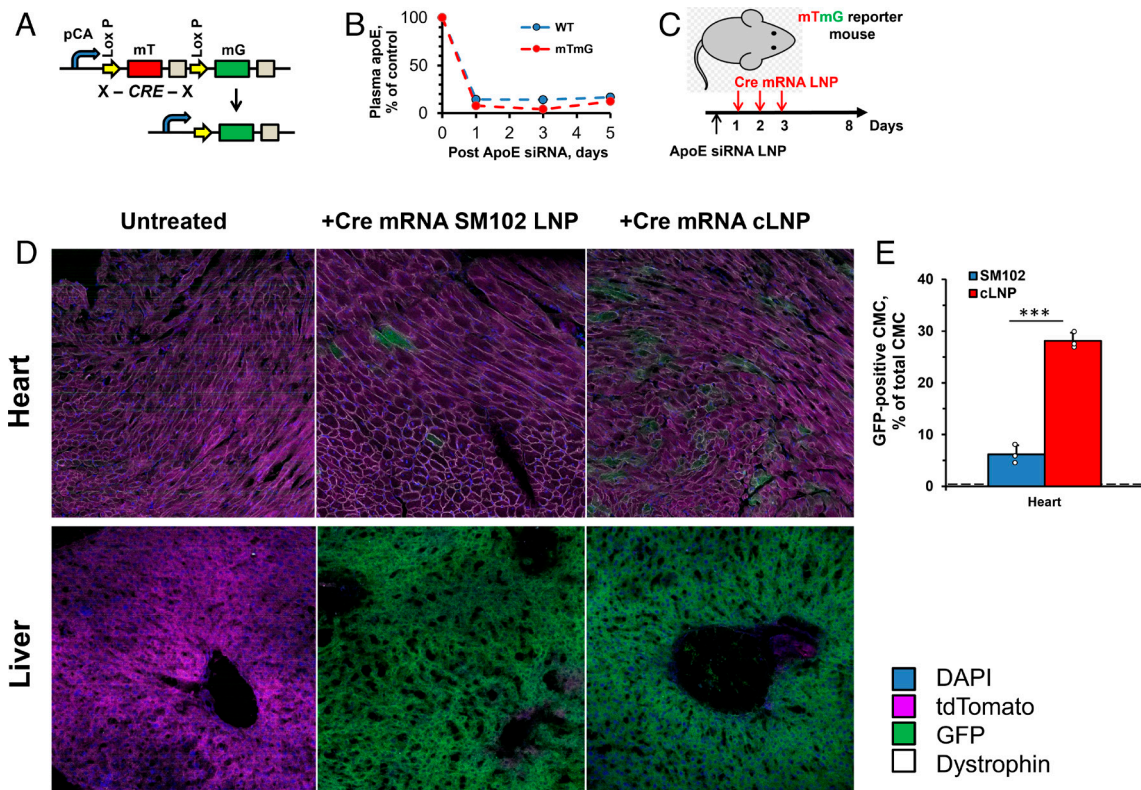


**Fig. 5.** Cre-Lox recombination by LNP/Cre recombinase mRNA indicates significant cLNP access to cardiomyocytes. (A) Schematic picture of Cre-Lox recombination. (B) Plasma apoE depletion by LNP/ApoE-siRNA treatment in WT and mTmG mice. (C) Treatment of mTmG mice with LNP. mTmG mice were pretreated with LNP/ApoE-siRNA and injected with 10  $\mu$ g of cLNP/Cre-mRNA or SM102/Cre-mRNA in 24, 48, and 72 h. Tissues were harvested at day 8 followed by confocal microscopy analysis. (D) Representative images of heart and liver tissues. Switch of tdTomato to GFP expression indicates recombined cells. Dystrophin staining of heart tissue outlines cardiomyocytes (white borders on heart images) and was used for proper identification. (E) Analysis of Cre-Lox recombination ( $n = 3, 4$  to 5 fields per heart,  $220 \pm 75$  CMC/field; analysis was done in a blind fashion). Fractions of GFP-positive cells of total cardiomyocyte number were calculated. The dashed line indicates the basal level in untreated mice. \*\*\* $P < 0.001$  ( $t$  test or two-way ANOVA with Tukey's post hoc test) cLNP vs. SM102-LNP.

delivery of inhibitory cargo to the cardiomyocytes. This proof-of-concept experiment bears several advantages. By working in animals with a healthy heart, we show that cLNP accumulation occurs in normal tissue without damaged or atypically permissive vasculature. Our imaging data show that cLNPs accumulate in the myocardial parenchyma and not the left ventricular chamber or blood vessels. We also observed relatively uniform uptake across the myocardium. Given the known reliance of myocardial nutrient delivery on the coronary vascular bed, this suggests that cLNP uptake occurs via coronary perfusion rather than transendocardial transport.

In order to quantify the relative contribution of ApoE to the biodistribution of cLNP, we implemented a PBPK model based on our previous model (54) and the reticuloendothelial system, largely composed of phagocytic cells in the liver and spleen, as the primary route of elimination of DDS is (55–57). The model suggests the following contributions of ApoE expression to the biodistribution pattern of cLNP, with a focus on effects on delivery to the heart. 1) ApoE promotes uptake of cLNP in the liver and spleen, contributing to 80 to 85% of the total uptake clearance in these organs. 2) ApoE reduces the affinity of cLNP for a saturable cardiac uptake pathway, with an estimated reduction in intrinsic uptake clearance of 10.5-fold in WT mice, compared to *ApoE*<sup>-/-</sup> mice.

Further, we show that systemic delivery is sufficient to achieve knockdown of an intracellular target, even of a protein as highly expressed as SERCA2. Although CMC SERCA2a is the major heart isoform that accounts for more than 99% of total cardiac SERCA (58), the finding does not preclude uptake of cLNP in noncardiomyocyte cell types within the heart. Elucidating cell-type affinity of cLNP or designing cell-type specific cargoes is a topic for future

work. Regardless, such cardiac tissue and CMC tropism obviate the need for more invasive delivery methods, such as intracoronary or intracardiac injection (59). Knockdown of SERCA2 led to direct effects on contractility in the cardiomyocyte. Finally, the versatility of siRNA affords numerous potential therapeutic opportunities. Therefore, cLNP delivery of siRNA represents a translational platform to interrogate disease-modifying cargoes. Moreover, we were able to deliver mRNA to a portion of CMCs. Further optimization, as has been observed with all LNP formulations, will be required.

The results of the present studies are important for basic research. The findings reported in this study inspire fundamental questions. What are the physiological and pathophysiological mechanism(s) and function(s) of this cLNP uptake phenomenon? It is plausible that apoE deficiency allows cLNP interaction with tentative binding site(s) in the cardiac vasculature, directly or via interaction with blood intermediary component(s). Identification of these molecules will enable cognizant cardiac drug targeting and shed light on a physiological transport phenomenon in the cardiovascular system. What natural purpose, if any, has cLNP exploited? What are the natural counterparts of cLNP—coronary lipids, receptors, or blood circulating entities? Uncovering the reasons for cLNP accumulation in the heart will not only reveal use of known or new transport machinery in the heart but may also present opportunities for further refinement of cLNP cardiotropism.

## Materials and Methods

**Antibodies and Proteins.** Monoclonal antibody MEC-13.3 toward murine PECAM was purchased from BD Biosciences (San Jose, CA). Antibodies to GAPDH (clone D4C6R; product #97166), ATP2A2/SERCA2 (product #4388),

$\beta$ -Actin (clone 8H10D10; product #3700), anti-mouse IgG, HRP linked (product #7076), anti-rabbit IgG, HRP linked (product #7074), anti-rabbit IgG (H + L) F(ab')<sub>2</sub> Fragment (Alexa Fluor 488 Conjugate) (product #4412), and anti-mouse IgG (H + L) F(ab')<sub>2</sub> Fragment (Alexa Fluor 594 Conjugate) (product #8890) were purchased from Cell Signaling Technology. Anti- $\alpha$ -Actinin (Sarcomeric) antibody produced in the mouse (product #A7811) was purchased from Sigma-Aldrich. Recombinant mouse 6His tagged apoE was purchased from Novoprotein Sci. Biotech. (Shanghai, China, product# CJ05).

**RNA Production, LNP Formulation, and TEM.** mRNAs were produced from a plasmid DNA template as described (60). To make modified nucleoside-containing mRNA, m<sup>1</sup> $\Psi$ -5'-triphosphate (TriLink) was incorporated instead of UTP. mRNAs were transcribed to contain 101 nucleotide-long poly(A) tails. Capping of mRNA was performed in concert with transcription through addition of a trinucleotide cap1 analog, CleanCap (TriLink). Cellulose-based purification of mRNA was performed as described (61). mRNAs were then checked on an agarose gel before storing at  $-20^{\circ}\text{C}$ . Purified mRNAs and poly(C) RNA (Sigma) were encapsulated in LNPs using a self-assembly process as previously described in which an aqueous solution of mRNA at acidic pH is rapidly mixed with a solution of lipids dissolved in ethanol (62). Prepared RNA or control poly(C) RNA (Sigma) were encapsulated in LNP using a self-assembly process as previously described in which an aqueous solution of RNA at acidic pH is rapidly mixed with a solution of lipids dissolved in ethanol (62). Formulations of cLNP were obtained from Acuitas Therapeutics (Vancouver, BC, Canada) and were used in earlier studies (43, 45). The composition of cLNP (proprietary to Acuitas Therapeutics (Vancouver, BC, Canada) described in US patent US10,221,127), and included phosphatidylcholine, cholesterol, and PEG-lipid in addition of ionizable lipid. A representative lot of cLNP had a diameter of  $77.43 \pm 0.58$  nm, PDI  $0.161 \pm 0.012$ ,  $\zeta$ -potential  $-7.95 \pm 0.50$  mV as measured by dynamic light scattering using a Zetasizer Nano ZS (Malvern Instruments Ltd, Malvern, UK) instrument. cLNP morphology was studied using a JEOL1010 transmission electron microscope (TEM), as described earlier (63). Carbon-coated 200-mesh copper grids were placed on a drop of the sample for 2 min and washed with Milli-Q water. Negative staining was done using 2% uranyl acetate. The stain was then wicked off with filter paper and the grids were dried and imaged at an acceleration voltage of 120 K. In comparative studies, we prepared LNPs with other ionizable lipids MC3, cKK-E12, C12-200, ALC-315, and DOTAP. Poly(C) RNA (Sigma) was encapsulated in LNPs using a self-assembly process in which an aqueous solution of RNA at pH = 4.0 is rapidly mixed with a solution of lipids dissolved in ethanol (62). The composition of LNPs reproduced a previously described formulation (62), which contains a corresponding ionizable cationic lipid, phosphatidylcholine, cholesterol, and PEG-lipid at molar ratio 50:10:38.5:1.5, respectively, and was encapsulated at an RNA to total lipid ratio of  $\sim 0.05$  (wt/wt). The characteristics of the LNPs used in the study are shown in *SI Appendix, Table S1*.

**LNP Radiolabeling.** We used <sup>3</sup>H and <sup>125</sup>I isotopes for nanoparticle labeling. Radiolabeling with <sup>3</sup>H was performed by addition of trace amount of <sup>3</sup>H-labeled cholesteryl hexadecyl ether (<sup>3</sup>H-CHE; PerkinElmer, Waltham, MA) to the ethanolic lipid mix prior to LNP formulation. Labeled LNP were stored at  $-80^{\circ}\text{C}$  before use. The iodination procedure was performed with formulated LNP in a glass tube coated with Pierce™ Iodination Reagent (1,3,4,6-tetrachloro-3 $\alpha$ ,6 $\alpha$ -diphenyl-glycoluril) in accordance with the manufacturer's recommendations (ThermoFisher, product #28600). Briefly, the reagent was dissolved in chloroform to 1 mg/mL and 100  $\mu\text{L}$  of the solution was added to a 5 mL glass tube, the reagent was dried out under the nitrogen flow, and tubes were kept in a desiccator. The iodination reaction was proceeded by incubation of 50  $\mu\text{L}$  of LNP at a concentration of 1 mg/mL RNA (20 mg/mL of lipid) in the glass tube in the presence of 150  $\mu\text{Ci}$  of Na<sup>125</sup>I (PerkinElmer) at room temperature for 15 min. Free iodine was removed by Zeba™ Spin Desalting Column (Thermo, product #89882). The iodine bound fraction of  $\sim 50$  to 60% was considered to be acceptable for further use. Freshly prepared <sup>125</sup>I-LNP were used for in vivo experiments due to potential leak of free iodine.

**Adult Cardiomyocyte Isolation and Cell Culture.** Adult rodent cardiomyocyte isolations were performed as previously described (64). Briefly, rats (for studies related to *SI Appendix, Fig. S8*) or mice (for studies related to Fig. 4) were anesthetized using isoflurane. Once the heart was excised, the aorta was cannulated and coronary arteries were flushed with cell isolation buffer (CIB, 130 mM NaCl,

1 mM sodium lactate, 5.4 mM KCl, 25 mM HEPES, 0.5 mM MgCl<sub>2</sub>·6H<sub>2</sub>O, 0.33 mM NaH<sub>2</sub>PO<sub>4</sub>, 22 mM dextrose, 20 mM creatine, and 10 U/L insulin) supplemented with 100 mM EGTA. The cannulated heart was connected to a Langendorff retrograde perfusion apparatus. The heart was rinsed with CIB without EGTA and then digested in a CIB containing type II collagenase (180 units/mL) and 50  $\mu\text{M}$  CaCl<sub>2</sub> until the heart was pale in appearance (8 to 12 min). The digested heart was minced, sheared using a transfer pipette, and centrifuged at 300 rpm for 2 min. The pellet was then serially resuspended in CIB containing 0.5 w/v% bovine serum albumin (BSA) and increasing concentrations of calcium (100  $\mu\text{M}$ , 400  $\mu\text{M}$ , 9 mM), with gravity settling between each solution. The final cardiomyocyte pellet was resuspended in adult cardiomyocyte media [Media 199 (ThermoFisher) supplemented with Primocin (InvivoGen), 25 mM HEPES, and Insulin-Transferrin-Selenium-Ethanolamide (Gibco)]. The medium was further supplemented with 25  $\mu\text{M}$  cytochalasin D if culture for greater than 12 h was required.

**Animals.** Animal work was performed in accordance with the University of Pennsylvania Institutional Animal Care and Use Committee and the Guide for the Care and Use of Laboratory Animals published by the US NIH. All mice strains were purchased from The Jackson Laboratory (Farmington, CT) and were 6 to 8 wk old if not indicated otherwise. Black mice C57BL/6 J are indicated as WT throughout the manuscript, ApoE knock-out mice B6.129P2-ApoE<sup>tm1Unc/J</sup> on C57BL/6 J background are indicated as ApoE<sup>-/-</sup>. mTmG reporter mice on C-57BL/65 black mice B6.129(Cg)-Gt(ROSA)26Sor<sup>tm4(ACTB-tdTomato,-EGFP)Lox/J</sup> are indicated as mTmG mice. Wistar rats (*Rattus norvegicus*) were obtained from Charles River Laboratories, Inc. (Boston, MA). Sprague Dawley (*Rattus norvegicus*) ApoE KO rats SD-ApoE<sup>tm1Sage</sup> were received from Envigo (Indianapolis, IN).

**Tissue Biodistribution and Pharmacokinetics of Radiolabeled cLNP.** For radiolabel-based tracing with <sup>125</sup>I or <sup>3</sup>H-CHE, LNP were injected in mice IV (1  $\mu\text{g}$  of RNA or  $\sim 20$   $\mu\text{g}$  lipid) retroorbitally. After 30 min, blood was drawn and the internal organs (liver, lung, kidney, heart, and spleen) were harvested, rinsed with saline, blotted dry, and weighed. Tissue radioactivity in organs and blood was determined in a Wallac 1470 Wizard™ gamma counter. Alternatively, for <sup>3</sup>H-CHE-labeled LNP, tissues were homogenized and lipids were extracted with hexane:2-propanol 3:2 mixture (v/v). Hexane upper layer was collected, dried, extracted lipids were reconstituted with scintillation liquid and radioactivity was measured in a LS 6500 Beckman beta-counter (65). Radioactivity values and weight of the samples were then used to calculate tissue uptake as percent of injected dose per gram of tissue (%ID/g). In experiments with empty LNP lipid equivalent to 1  $\mu\text{g}$  of RNA-LNP (i.e. 20  $\mu\text{g}$  of lipid) was injected. In experiments with rats, 10  $\mu\text{g}$  of <sup>125</sup>I-RNA-LNP was injected via the tail vein. In pharmacokinetics experiments, animals were killed at 5, 15, 30, 60, and 120 min postinjection. In experiments with rats, anesthesia was induced with 5% isoflurane, animals were intubated and ventilated, and sedation was maintained with 3% isoflurane. Injection of <sup>125</sup>I-LNP was performed via the tail vein and allowed to circulate for 30 min. Blood was collected from the inferior vena cava, and the heart, lung, liver, kidney, and spleen were harvested.

**Tissue Biodistribution of Ionizable Lipid by LC-MS/MS Quantitation.** C57BL/6 J and B6.129P2-ApoE<sup>tm1Unc/J</sup> mice were injected with 0.05 mg/kg of cLNP ( $\sim 1$   $\mu\text{g}$  RNA/animal) via the lateral tail vein. At 0.5 h and 4 h postdose, blood was drawn prior to cardiac perfusion with saline for 10 min. Organs were collected, weighed, and snap-frozen in liquid nitrogen pending aminolipid analysis. The cLNP aminolipid was analyzed in heart and liver samples by a 1:9 tissue:solvent (50/40/10 [0.1% formic acid in 50/50 methanol/acetonitrile]/[10 mM ammonium formate with 0.2% formic acid] / [DMF]) homogenization. After homogenization, 25  $\mu\text{L}$  of homogenate was mixed with 25  $\mu\text{L}$  of control plasma and 25  $\mu\text{L}$  of 100 ng/mL of deuterated internal standard lipid. The sample was then crashed with 400  $\mu\text{L}$  of extraction solvent (0.1% formic acid in acetonitrile:methanol 1:1). 150  $\mu\text{L}$  of the supernatant was removed to a clean 96-well injection plate and centrifuged at 3,000  $\times g$  for 5 min prior to analysis. Samples were quantitated against a freshly prepared calibration curve using a best fit regression from 20.0 to 50,000 ng/g. Chromatography was performed on a Waters XBridge BEH C8 (2.1  $\times$  30 mm) column at a flow rate of 0.5 mL/min. A gradient method was used starting at 85% B (0.1% formic acid in 1:1 methanol:acetonitrile) for 18 s and then ramping to 98% B over 42 s. This composition was held for 1.0 min before being returned to starting conditions and re-equilibration to 15% A (10 mM ammonium formate in water with 0.2% formic acid). The peak area ratio of the

aminolipid and internal standard was plotted against the standard concentrations and a best fit regression (linear or quadratic) was used to quantitate the amount of aminolipid in the samples.

### Physiologically Based Pharmacokinetic (PBPK) Modeling of cLNP.

**Whole-body model structure.** The PBPK model utilized here was adapted from our recent publication describing model development for vascular targeted LNP in mice (54). Briefly, key organs of distribution (blood, lungs, heart, kidneys, spleen, liver) were linked in an anatomically relevant manner using physiologic parameters for a 25 g mouse (*SI Appendix, Fig. S10 and Table S2*).

**Tissue submodel.** Models were created to describe the intraorgan distribution patterns for all tissues with pharmacokinetic data (lungs, heart, kidneys, spleen, liver). In general, cLNP entered and left the vascular space of each organ by the relevant organ blood flow. Organs were divided into vascular and intracellular compartments, with physiologically relevant volumes (*SI Appendix, Table S2*). Four unique model structures were built, based on distribution patterns observed in each organ. Class 1 (Lungs, Kidneys): Cellular uptake modeled using a first-order tissue uptake clearance (*SI Appendix, Fig. S11A*). Class 2 (Heart): Cellular uptake modeled using a Michaelis-Menten uptake clearance (*SI Appendix, Fig. S11B*). Class 3 (Spleen): Cellular uptake modeled using parallel first-order uptake clearances, with one being dependent on the presence of ApoE (*SI Appendix, Fig. S11C*). Class 4 (Liver): Cellular uptake modeled using parallel uptake clearances, with a first-order, ApoE-dependent pathway and a Michaelis-Menten, ApoE-independent pathway (*SI Appendix, Fig. S11D*).

**Datasets for modeling.** Data used for model development included the following: 1) pharmacokinetics and biodistribution in WT mice, obtained from our previous publication (43), and 2) pharmacokinetics and biodistribution in *ApoE*<sup>-/-</sup> mice, depicted in the main text of this manuscript.

**Model fitting.** All data were simultaneously fit to the pharmacokinetics and biodistribution model using ADAPT 5 (66). Model performance was assessed by visual inspection of goodness-of-fit and reliability of parameter estimates.

**Autoradiography.** 20  $\mu\text{g}$  of <sup>125</sup>I-cLNP was injected retroorbitally in C57BL/6 J and B6.129P2-ApoE<sup>tm1.1unt/J</sup> mice. Hearts were harvested in 30 min, washed, and fixed overnight in 4% paraformaldehyde. Fixed hearts were cut on four 2-mm slices and exposed on X-ray Film for 72 h.

**Apolipoprotein E Depletion.** For transient depletion of apoE in mice, siRNA to murine ApoE was used (Dharmacon, A Horizon Discovery Group Company; ON-TARGETplus siRNA; product J-040885-06). siRNA was complexed in LNP using InvivoFectamine 3.0 Reagent (Invitrogen, #IVF3001) in accordance with the manufacturer's recommendation. Sixty  $\mu\text{g}$  of ApoE siRNA-LNP was injected in the WT mouse. To confirm apoE depletion, the level of plasma apoE was measured by Mouse Apolipoprotein E ELISA (Abcam, product ab215086). In 24 h, plasma apoE concentration dropped by at least 70% from normal (67) 123.0  $\pm$  6.1  $\mu\text{g}/\text{mL}$  to 34.7  $\pm$  5.2  $\mu\text{g}/\text{mL}$  and was stable for 3 d followed by an increase (*SI Appendix, Fig. S2B*).

**Confocal Microscopy Studies of LNP Accumulation in the Heart.** cLNP were labeled with PKH26 red fluorescent dye (Sigma) and injected retroorbitally in mice. In some experiments 10 min before organ harvesting 40  $\mu\text{g}$  of Alexa Fluor 647-labeled anti-PECAM monoclonal antibody (MEC13.3; BD Pharmingen) was injected for in vivo staining of blood vessels. Organs were harvested, frozen in O.C.T. Compound (Fisher HealthCare), and cryosectioned using cryostat Leica CM 1950 (Leica BioSystems, Nussloch, Germany). Cardiomyocytes were visualized with rabbit antibodies to mouse dystrophin (Abcam, product #15277) and Alexa-647-labeled anti-rabbit secondary antibodies (Invitrogen, ThermoFisher). Finally, samples were mounted using ProLong Gold Antifade Reagent with DAPI (Molecular Probes, ThermoFisher). Microscopy studies were performed on a confocal laser scanning microscope Leica TCS-SP8 (Leica, Germany) using HC PLAPO CS2 63 $\times$ /1.40 Oil objective and 488/552/638 lasers. Images were processed using Volocity 6.3 Cellular Imaging & Analysis.

**Delivery of LNP-mRNA Cre Recombinase and GFP Expression in CMC.** Reporter mice B6.129(Cg)-Gt(ROSA)26Sor<sup>tm4(ACTB-ttdTomato,-EGFP)LoxP/J</sup> (mTmG) on C-57BL/65 black mice background were used in the study. First, animals received retro-orbital injections of 60  $\mu\text{g}$  ApoE siRNA-LNP as described above. In 24 h plasma apoE level was measured and the protein depletion was confirmed. One, 2, and 3 d post-siRNA injection, mTmG mice were injected with 10  $\mu\text{g}$  of cLNPs

or control SM102 LNPs containing Cre recombinase mRNA. On Day 8, animals were killed, and organs were harvested (Fig. 5A-C). Confocal microscopy studies were performed as described above using a 20 $\times$  objective. Dystrophin staining was used for outlining individual CMCs. We performed a quantitative analysis of the Cre images with 4 to 5 fields per heart in each animal group ( $n = 3$ ). On average 220  $\pm$  75 CMCs per field were analyzed. Each image was deidentified by labeling with randomly generated numbers, and two blinded scorers counted the number of GFP-positive vs. tdTomato-positive CMCs per image.

**In Vitro Uptake of LNP.** Adult rat cardiomyocytes were incubated with varying concentrations of cLNP loaded with GFP mRNA. After 12 h, cells were washed with phosphate-buffered saline (PBS) and counterstained with NucBlue (Hoechst 33342, Invitrogen). Cells were imaged on a Nikon Ti-U inverted fluorescence microscope using Photometrics CoolSNAP HQ<sup>2</sup>. Images were analyzed for fluorescence intensity per cell relative to background using ImageJ.

**SDS-Polyacrylamide Gel Electrophoresis and Western Blotting.** Samples were mixed with sample buffer for SDS-PAGE and then were subjected to 4 to 15 % gradient SDS-electrophoresis. Protein, either from cells or pulverized tissues, was lysed using RIPA Buffer (CellSignal Technology) with protease inhibitor cocktail (CellSignal Technology). Protein quantity was verified using the BCA Protein Assay Kit (Pierce). Protein was combined with 4 $\times$  Laemmli protein sample buffer (Bio-Rad) and 2-Mercaptoethanol and boiled for 6 min. Samples were run on a 4 to 20% Criterion TGX gel (Bio-Rad) and transferred to a nitrocellulose membrane (Bio-Rad). Membranes were blocked using the Pierce Protein Free Blocking Buffer (ThermoFisher) for 1 h. Primary antibodies were shaken over the membrane overnight at 4  $^{\circ}\text{C}$ . Membranes were washed three times with TBST (CellSignal Technology) and secondary antibodies were added for 1 h prior to another three washes with TBST. SuperSignal West Femto Maximum Sensitivity Substrate (ThermoFisher) was added to the membranes and chemiluminescence was immediately imaged using ImageQuant LAS (GE Healthcare).

**Dynamic Light Scattering.** The effective diameter of the prepared particles and polydispersity index (PDI) was measured by Zetasizer Nano ZSP (Malvern Instruments Ltd., Malvern, UK).

**Validation of siATP2A2 siRNA.** Two siRNAs were used, a scrambled pool of nontargeting siRNAs (ON-Targetplus, Horizon Discovery Biosciences) or siRNA targeting ATP2A2 (ON-Targetplus, Horizon Discovery Biosciences, sequence: GACUUACUAGUUAGAAUUU). Human iPS cardiomyocytes (Ncardia, (Leiden, The Netherlands) Ncyte vCardiomyocytes) were obtained commercially without identifying information prior to our use and were incubated with 25 pmol siRNA in Lipofectamine RNAiMAX (Invitrogen) for up to 48 h. Cells were washed and used for downstream experiments. For gene expression analysis, RNA was isolated using Qiazol (Qiagen) and RNeasy Kit (Qiagen). Reverse transcription was performed using the High-Capacity cDNA Reverse Transcription Kit (Applied Biosystems), and qPCR was performed using Luna Universal qPCR Master Mix (New England Biolabs) and Applied Biosystems QuantStudio 6 flex. Data were analyzed using the  $\Delta\Delta\text{Ct}$  method. For immunofluorescence, iPS cardiomyocytes were fixed with 4% paraformaldehyde for 15 min, permeabilized with 0.1% Triton-X, and nonspecific binding blocked with 5% BSA. Primary and secondary antibodies were incubated for 1 h each with three PBS washes in between. Cells were counterstained with DAPI and imaged using a Nikon Ti-U inverted fluorescence microscope. For relative contraction and calcium analysis, iPS-CMs were initially seeded on MatTek 35 mm glass bottom dishes incubated with siRNA as above. For calcium studies, cells were incubated with 1  $\mu\text{M}$  Fura-2 AM (Invitrogen) for 30 min and then allowed to de-esterify for 30 min. Data were acquired using the MultiCell High Throughput System with CytoMotion software and analyzed using CytoSolver Transient Analysis Tool (IonOptix).

**Delivery of LNP-siATP2A2 and SERCA2a Expression.** Mice received retro-orbital injections of 10  $\mu\text{g}$  cLNP-scrambled or cLNP-siATP2A2 RNA. At 1, 3, or 5 d following injection, mice were anesthetized using isoflurane, and hearts were excised and weighed. Tibia lengths were measured. Hearts were halved along the short axis. Half was fixed with paraformaldehyde and subsequently embedded in paraffin and stained with hematoxylin and eosin. To determine cardiomyocyte cross-sectional area, heart sections were stained with wheat germ agglutinin, Texas Red conjugate (Invitrogen), and DAPI to visualize the surface of

cell membranes and nuclei, respectively. The other half was flash-frozen and mechanically pulverized for downstream protein isolation (see below). Image analyses were performed on ImageJ. For contractility analysis, whole hearts were excised, and cardiomyocytes were isolated as above. Media was changed to adult cardiomyocyte media without Cytochalasin D. Contractility data were acquired using the MultiCell High Throughput System. Briefly, cells were kept at 37 °C, and a high-speed camera (MyoCam-S3, IonOptix) was used to capture real-time sarcomere length via Fourier transform (IonWizard, IonOptix). Cells were paced using a MyoPacer at 1 Hz and data were captured for 10 s. Contractility transient data were analyzed using CytoSolver Transient Analysis Tool (IonOptix). Slides were rehydrated; then, antigens were retrieved using SignalStain Citrate Unmasking Solution (CellSignaling Technology) in a pressure cooker for 15 min. To visualize SERCA2a expression, heart sections were permeabilized using 0.1% Triton X and blocked with 3% bovine serum albumin. Slides were incubated overnight at 4 °C in primary antibodies [1:100 ATP2A2/SERCA2 (D51B11) Rabbit mAb (CellSignaling Technology) and 1:100 Anti- $\alpha$ -Actinin (Sarcomeric) antibody, Mouse monoclonal (Sigma)]. Following three washes with PBS, slides were incubated in secondary antibodies for 1 h and counterstained with DAPI. Images were acquired on a Zeiss LSM 710 laser scanning confocal microscope. Mean fluorescence intensity per nuclei count was calculated for 3 to 5 images per animal.

**Toxicity Studies.** To test the proinflammatory response to LNP, we measured the plasma level of 13 inflammatory cytokines at 24, 48, and 72 h after intravenous administration of 10  $\mu$ g of cLNP or MC3 LNP in *ApoE*<sup>-/-</sup> mice. Lipopolysaccharide (LPS) was injected at a concentration of 2 mg/kg and used in some assays as a positive control. Plasma level of cytokines was measured on a BD Beckman

CytoFlex LX 6 laser system (BD Biosciences, San Jose, CA) using the LEGENDplex Mouse Inflammation Panel (13-plex) and LEGENDplex software (BioLegend, San Diego, CA; product # 740150). This panel included 13 proinflammatory cytokines IL-1 $\alpha$ , IL-1 $\beta$ , IL-6, IL-10, IL-12p70, IL-17A, IL-23, IL-27, MCP-1, IFN- $\beta$ , IFN- $\gamma$ , TNF- $\alpha$ , and GM-CSF.

**Data, Materials, and Software Availability.** All methods, protocols, reagents, and study data are available in the article and [supporting information](#).

**ACKNOWLEDGMENTS.** We thank Drs. Elena Atochina-Vasserman and Jaclynn Meshanni for the assistance with toxicity assays. This work was funded by NIH Grant RO1 HL155106 (V.R.M.).

Author affiliations: <sup>a</sup>Department of Systems Pharmacology and Translational Therapeutics, Perelman School of Medicine, University of Pennsylvania, Philadelphia, PA 19104; <sup>b</sup>Acuitas Therapeutics, Vancouver, BC V6T 1Z3, Canada; <sup>c</sup>Cardiovascular Institute, Perelman School of Medicine, Division of Cardiology, University of Pennsylvania, Philadelphia, PA 19104; <sup>d</sup>Division of Cardiothoracic Surgery, Hospital of the University of Pennsylvania, Philadelphia, PA 19104; <sup>e</sup>Department of Pharmaceutical Sciences, School of Pharmacy, Temple University, Philadelphia, PA 19140; <sup>f</sup>Division of Infectious Diseases, Perelman School of Medicine, University of Pennsylvania, Philadelphia, PA 19104; <sup>g</sup>Department of Bioengineering, University of Pennsylvania, Philadelphia, PA 19104; and <sup>h</sup>Department of Medicine, Division of Pulmonary, Allergy, and Critical Care Medicine, Perelman School of Medicine, University of Pennsylvania, Philadelphia, PA 19104

Author contributions: V.V.S., B.W.L., J.W.M., A.H., K.M., J.S.B., V.A.F., P.A., K.B.M., D.W., and V.R.M. designed research; V.V.S., B.W.L., A.H., R.Y.K., T.I.S., E.A., O.A.M.-C., E.D.H., T.V.B., J.N., T.E.P., D.M.E., R.P., B.L.M., S.C.S., and S.A.W. performed research; Y.K.T., H.P., M.-G.A., N.P., H.M., R.R., M.J.M., and B.L.M. contributed new reagents/analytic tools; V.V.S., B.W.L., J.W.M., R.Y.K., P.M.G., H.P., M.-G.A., H.M., T.I.S., E.A., O.A.M.-C., E.D.H., T.V.B., J.N., T.E.P., D.M.E., R.P., S.C.S., S.A.W., P.A., K.B.M., D.W., and V.R.M. analyzed data; and V.V.S., Y.K.T., B.W.L., J.W.M., P.M.G., N.P., M.J.M., V.A.F., K.B.M., D.W., and V.R.M. wrote the paper.

1. C. W. Tsao *et al.*, Heart disease and stroke statistics-2023 update: A report from the American Heart Association. *Circulation* **147**, e93 (2023).
2. P. A. Heidenreich *et al.*, Forecasting the impact of heart failure in the United States: A policy statement from the American Heart Association. *Circ. Heart Fail.* **6**, 606-619 (2013).
3. C. W. Yancy *et al.*, 2017 ACC/AHA/HFSA Focused Update of the 2013 ACCF/AHA guideline for the management of heart failure: A report of the American college of cardiology/american heart association task force on clinical practice guidelines and the heart failure society of America. *Circulation* **136**, e137 (2017).
4. J. S. Hulot, K. Ishikawa, R. J. Hajjar, Gene therapy for the treatment of heart failure: Promise postponed. *Eur. Heart J.* **37**, 1651-1658 (2016).
5. P. Das, R. A. Thandavarayan, K. Watanabe, R. Velayutham, S. Arumugam, Right ventricular failure: A comorbidity or a clinical emergency?. *Heart Fail. Rev.* **27**, 1779-1793 (2022).
6. M. J. W. Evers *et al.*, Delivery of modified mRNA to damaged myocardium by systemic administration of lipid nanoparticles. *J. Control. Release.* **343**, 207-216 (2022).
7. W. C. Aird, Phenotypic heterogeneity of the endothelium: I. Structure, function, and mechanisms. *Circ. Res.* **100**, 158-173 (2007).
8. M. A. Laflamme, C. E. Murry, Heart regeneration. *Nature* **473**, 326-335 (2011).
9. Q. Yang, J. Fang, Z. Lei, J. P. G. Sluijter, R. Schifflers, Repairing the heart: State-of-the-art delivery strategies for biological therapeutics. *Adv. Drug Deliv. Rev.* **160**, 1-18 (2020).
10. K. Paunovska *et al.*, A direct comparison of in vitro and in vivo nucleic acid delivery mediated by hundreds of nanoparticles reveals a weak correlation. *Nano Lett.* **18**, 2148-2157 (2018).
11. G. de Couto, Macrophages in cardiac repair: Environmental cues and therapeutic strategies. *Exp. Mol. Med.* **51**, 1-10 (2019).
12. H. Kim *et al.*, Cardiac-specific delivery by cardiac tissue-targeting peptide-expressing exosomes. *Biochem. Biophys. Res. Commun.* **499**, 803-808 (2018).
13. Q. Li *et al.*, Engineering extracellular vesicles with platelet membranes fusion enhanced targeted therapeutic angiogenesis in a mouse model of myocardial ischemia reperfusion. *Theranostics* **11**, 3916-3931 (2021).
14. X. Liu *et al.*, In vitro and in vivo evaluation of liposomes modified with polypeptides and red cell membrane as a novel drug delivery system for myocardium targeting. *Drug Deliv.* **27**, 599-606 (2020).
15. K. I. Mentkowski, J. K. Lang, Exosomes engineered to express a cardiomyocyte binding peptide demonstrate improved cardiac retention *in vivo*. *Sci. Rep.* **9**, 10041 (2019).
16. L. Saludas *et al.*, Extracellular vesicle-based therapeutics for heart repair. *Nanomaterials* **11**, 570 (2021).
17. M. Shin *et al.*, Targeting protein and peptide therapeutics to the heart via tannic acid modification. *Nat. Biomed. Eng.* **2**, 304-317 (2018).
18. A. Vandergriff *et al.*, Targeting regenerative exosomes to myocardial infarction using cardiac homing peptide. *Theranostics* **8**, 1869-1878 (2018).
19. J. J. Wright, A. C. Powers, D. B. Johnson, Endocrine toxicities of immune checkpoint inhibitors. *Nat. Rev. Endocrinol.* **17**, 389-399 (2021).
20. A. Cannata, H. Ali, G. Sinagra, M. Giacca, Gene therapy for the heart lessons learned and future perspectives. *Circ. Res.* **126**, 1394-1414 (2020).
21. L. R. Baden *et al.*, Efficacy and safety of the mRNA-1273 SARS-CoV-2 vaccine. *N. Engl. J. Med.* **384**, 403-416 (2021).
22. M. J. Hogan, N. Pardi, mRNA vaccines in the COVID-19 pandemic and beyond. *Annu. Rev. Med.* **73**, 17-39 (2022).
23. J. D. Gillmore *et al.*, CRISPR-Cas9 in vivo gene editing for transthyretin amyloidosis. *N. Engl. J. Med.* **385**, 493-502 (2021).
24. A. Mullard, Pfizer's COVID-19 vaccine secures first full FDA approval. *Nat. Rev. Drug Discov.* **20**, 728 (2021).
25. X. Hou, T. Zaks, R. Langer, Y. Dong, Lipid nanoparticles for mRNA delivery. *Nat. Rev. Mater.* **6**, 1078-1094 (2021).
26. M. Cheraghi, B. Negahdari, H. Daraee, A. Eatemadi, Heart targeted nanoliposomal/nanoparticles drug delivery: An updated review. *Biomed. Pharmacother.* **86**, 316-323 (2017).
27. H. L. Sullivan, N. C. Gianneschi, K. L. Christman, Targeted nanoscale therapeutics for myocardial infarction. *Biomater. Sci.* **9**, 1204-1216 (2021).
28. S. Marchio, R. L. Sidman, W. Arap, R. Pasqualini, Brain endothelial cell-targeted gene therapy of neurovascular disorders. *EMBO Mol. Med.* **8**, 592-594 (2016).
29. P. M. Glassman *et al.*, Targeting drug delivery in the vascular system: Focus on endothelium. *Adv. Drug Deliv. Rev.* **157**, 96-117 (2020).
30. K. Paunovska, D. Loughrey, J. E. Dahlman, Drug delivery systems for RNA therapeutics. *Nat. Rev. Genet.* **23**, 265-280 (2022).
31. Q. Cheng *et al.*, Selective organ targeting (SORT) nanoparticles for tissue-specific mRNA delivery and CRISPR-Cas gene editing. *Nat. Nanotechnol.* **15**, 313-320 (2020).
32. S. Scalzo *et al.*, Ionizable lipid nanoparticle-mediated delivery of plasmid DNA in cardiomyocytes. *Int. J. Nanomed.* **17**, 2865-2881 (2022).
33. D. J. Siegwart *et al.*, Combinatorial synthesis of chemically diverse core-shell nanoparticles for intracellular delivery. *Proc. Natl. Acad. Sci. U. S. A.* **108**, 12996-13001 (2011).
34. H. Zhang *et al.*, Rational design of anti-inflammatory lipid nanoparticles for mRNA delivery. *J. Biomed. Mater. Res. A* **110**, 1101-1108 (2022).
35. L. M. Kranz *et al.*, Systemic RNA delivery to dendritic cells exploits antiviral defence for cancer immunotherapy. *Nature* **534**, 396-401 (2016).
36. C. Krienke *et al.*, A noninflammatory mRNA vaccine for treatment of experimental autoimmune encephalomyelitis. *Science* **371**, 145-153 (2021).
37. S. Liu *et al.*, Membrane-destabilizing ionizable phospholipids for organ-selective mRNA delivery and CRISPR-Cas gene editing. *Nat. Mater.* **20**, 701-710 (2021).
38. C. Niemietz, O. Nadzemova, A. Zibert, H. H. Schmidt, APOE polymorphism in ATTR amyloidosis patients treated with lipid nanoparticle siRNA. *Amyloid* **27**, 45-51 (2020).
39. F. Sebastiani *et al.*, Apolipoprotein E binding drives structural and compositional rearrangement of mRNA-containing lipid nanoparticles. *ACS Nano* **15**, 6709-6722 (2021).
40. A. J. Silva Sanchez *et al.*, Universal barcoding predicts in vivo ApoE-independent lipid nanoparticle delivery. *Nano Lett.* **22**, 4822-4830 (2022).
41. S. A. Dilliard, Q. Cheng, D. J. Siegwart, On the mechanism of tissue-specific mRNA delivery by selective organ targeting nanoparticles. *Proc. Natl. Acad. Sci. U. S. A.* **118**, e2109256118 (2021).
42. D. Chen, N. Parayath, S. Ganesh, W. Wang, M. Amiji, The role of apolipoprotein- and vitronectin-enriched protein corona on lipid nanoparticles for in vivo targeted delivery and transfection of oligonucleotides in murine tumor models. *Nanoscale* **11**, 18806-18824 (2019).
43. H. Parhiz *et al.*, PECAM-1 directed re-targeting of exogenous mRNA providing two orders of magnitude enhancement of vascular delivery and expression in lungs independent of apolipoprotein E-mediated uptake. *J. Control. Release.* **291**, 106-115 (2018).
44. J. Ramos da Silva *et al.*, Single immunizations of self-amplifying or non-replicating mRNA-LNP vaccines control HPV-associated tumors in mice. *Sci. Transl. Med.* **15**, eabn3464 (2023).
45. N. Pardi, H. Muramatsu, D. Weissman, K. Kariko, In vitro transcription of long RNA containing modified nucleosides. *Methods Mol. Biol.* **969**, 29-42 (2013).
46. G. Lo Sasso *et al.*, The ApoE(-/-) mouse model: A suitable model to study cardiovascular and respiratory diseases in the context of cigarette smoke exposure and harm reduction. *J. Transl. Med.* **14**, 146 (2016).

47. L. T. Johnson *et al.*, Lipid nanoparticle (LNP) chemistry can endow unique in vivo RNA delivery fates within the liver that alter therapeutic outcomes in a cancer model. *Mol. Pharm.* **19**, 3973–3986 (2022).
48. X. Yu *et al.*, Hydrophobic optimization of functional poly(TPAE-co-suberoyl chloride) for extrahepatic mRNA delivery following intravenous administration. *Pharmaceutics* **13**, 1914 (2021).
49. J. G. Rurik *et al.*, CAR T cells produced in vivo to treat cardiac injury. *Science* **375**, 91–96 (2022).
50. V. Anttila *et al.*, Synthetic mRNA encoding VEGF-A in patients undergoing coronary artery bypass grafting: Design of a phase 2a clinical trial. *Mol. Ther. Methods Clin. Dev.* **18**, 464–472 (2020).
51. T. J. Antes *et al.*, Targeting extracellular vesicles to injured tissue using membrane cloaking and surface display. *J. Nanobiotechnol.* **16**, 61 (2018).
52. H. Kim *et al.*, Improved cardiac-specific delivery of RAGE siRNA within small extracellular vesicles engineered to express intense cardiac targeting peptide attenuates myocarditis. *Mol. Ther.* **24**, 1024–1032 (2021).
53. M. Liu *et al.*, Bispecific antibody inhalation therapy for redirecting stem cells from the lungs to repair heart injury. *Adv. Sci. (Weinh.)* **8**, 2002127 (2020).
54. H. Parhiz *et al.*, Physiologically based modeling of LNP-mediated delivery of mRNA in the vascular system. *Mol. Ther. Nucleic Acids* **35**, 102175 (2024).
55. A. C. Anselmo *et al.*, Delivering nanoparticles to lungs while avoiding liver and spleen through adsorption on red blood cells. *ACS Nano* **7**, 11129–11137 (2013).
56. E. Lazaro-Ibanez *et al.*, Selection of fluorescent, bioluminescent, and radioactive tracers to accurately reflect extracellular vesicle biodistribution in vivo. *ACS Nano* **15**, 3212–3227 (2021).
57. N. J. Reyes, E. G. O’Koren, D. R. Saban, New insights into mononuclear phagocyte biology from the visual system. *Nat. Rev. Immunol.* **17**, 322–332 (2017).
58. L. Lipskaia *et al.*, Expression of sarco (endo) plasmic reticulum calcium ATPase (SERCA) system in normal mouse cardiovascular tissues, heart failure and atherosclerosis. *Biochim. Biophys. Acta* **1843**, 2705–2718 (2014).
59. I. C. Turnbull *et al.*, Myocardial delivery of lipidoid nanoparticle carrying modRNA induces rapid and transient expression. *Mol. Ther.* **24**, 66–75 (2016).
60. I. Tombacz *et al.*, Highly efficient CD4+ T cell targeting and genetic recombination using engineered CD4+ cell-homing mRNA-LNPs. *Mol. Ther.* **29**, 3293–3304 (2021).
61. M. Baidersdorfer *et al.*, A facile method for the removal of dsRNA contaminant from in vitro-transcribed mRNA. *Mol. Ther.* **15**, 26–35 (2019).
62. M. A. Maier *et al.*, Biodegradable lipids enabling rapidly eliminated lipid nanoparticles for systemic delivery of RNAi therapeutics. *Mol. Ther.* **21**, 1570–1578 (2013).
63. M. Khoshnejad, H. Parhiz, V. V. Shuvaev, I. J. Dmochowski, V. R. Muzykantov, Ferritin-based drug delivery systems: Hybrid nanocarriers for vascular immunotargeting. *J. Control. Release.* **282**, 13–24 (2018).
64. C. Y. Chen *et al.*, Depletion of vasohibin 1 speeds contraction and relaxation in failing human cardiomyocytes. *Circ. Res.* **127**, e14 (2020).
65. M. D. Wang, V. Franklin, Y. L. Marcel, In vivo reverse cholesterol transport from macrophages lacking ABCA1 expression is impaired. *Arterioscler. Thromb. Vasc. Biol.* **27**, 1837–1842 (2007).
66. D. Z. D’Argenio, A. Schumitzky, X. Wang, *ADAPT 5 User’s Guide: Pharmacokinetic/Pharmacodynamic Systems Analysis Software* (Biomedical Simulations Resource, Los Angeles, CA, 2009).
67. H. Wientgen *et al.*, Subphysiologic apolipoprotein E (ApoE) plasma levels inhibit neointimal formation after arterial injury in ApoE-deficient mice. *Arterioscler. Thromb. Vasc. Biol.* **24**, 1460–1465 (2004).